JGR Biogeosciences

RESEARCH ARTICLE
10.1029/2021JG006524

Considerable Uncertainties in Simulating Land Carbon Sinks Induced by Different Precipitation Products

Meirong Wang[1], Jun Wang[2,3], Qixiang Cai[4], Ning Zeng[5], Xuehe Lu[6], Ruqi Yang[4,7], Fei Jiang[2,3], Hengmao Wang[2,3], and Weimin Ju[2,3]

[1]Joint Center for Data Assimilation Research and Applications/Key Laboratory of Meteorological Disaster, Ministry of Education/Joint International Research Laboratory of Climate and Environment Change (ILCEC)/Collaborative Innovation Center ON Forecast and Evaluation of Meteorological Disasters, Nanjing University of Information Science and Technology, Nanjing, China, [2]International Institute for Earth System Science, Nanjing University, Nanjing, China, [3]Jiangsu Provincial Key Laboratory of Geographic Information Science and Technology, Key Laboratory for Land Satellite Remote Sensing Applications of Ministry of Natural Resources, School of Geography and Ocean Science, Nanjing University, Nanjing, China, [4]State Key Laboratory of Numerical Modelling for Atmospheric Sciences and Geophysical Fluid Dynamics, Institute of Atmospheric Physics, Chinese Academy of Sciences, Beijing, China, [5]Department of Atmospheric and Oceanic Science and Earth System Interdisciplinary Center, University of Maryland, College Park, MD, USA, [6]School of Geography Science and Geomatics Engineering, Suzhou University of Science and Technology, Suzhou, China, [7]College of Earth and Planetary Sciences, University of Chinese Academy of Sciences, Beijing, China

Abstract

Precipitation, a key determinant of soil moisture variations, plays an important role in regulating terrestrial carbon fluxes on multiple time scales. It is a critical meteorological forcing to drive terrestrial biosphere model (TBM), however, with a large uncertainty itself. We here investigated to what extent precipitation alone can cause uncertainties of model-simulated carbon flux from terrestrial ecosystems to atmosphere (F_{TA}), based on eight precipitation products and a TBM, VEGAS. We find that the pattern of uncertainties in simulated F_{TA} obviously differs from the pattern of discrepancies in precipitation, owing to divergent water sensitivities of vegetation over different regions. Globally, the uncertainty in F_{TA} can be up to approximately 40.73% of the uncertainty in TRENDYv6 multi-model simulated F_{TA} which is caused by model structural and parameter uncertainty. A good linear relationship emerges between global area-averaged land climatological annual precipitation and simulated total F_{TA} with the slope of -0.0040 PgC yr^{-1} per mm yr^{-1} ($p = 0.03$; negative for carbon sink), where 70% is explained by the sensitivity over extra-tropical Northern Hemisphere (NH). For seasonal cycle, compared to nearly constant inter-precipitation spreads over tropics plus extra-tropical southern hemisphere (Trop + SH), uncertainties in corresponding simulated F_{TA} show obvious seasonal differences with the relatively larger uncertainties in March-April-May (MAM) and August-September-October (ASO). For interannual variability, uncertainties in simulated total F_{TA} are, albeit smaller, nonnegligible, which are 40.61% (global), 38.17% (Trop + SH), and 29.63% (NH) of the TRENDYv6 inter-model uncertainty, respectively. Therefore, generating better global precipitation product is important for reducing the uncertainty in simulating terrestrial carbon sinks.

Plain Language Summary

Precipitation, a key forcing in terrestrial biosphere model (TBM), has a large uncertainty itself. We here used eight land precipitation products to run TBM VEGAS and explored the resulting uncertainties in simulating carbon flux from terrestrial ecosystems to atmosphere (F_{TA}) on climatology, seasonal cycle, and interannual variability. In climatology, the uncertainty in global F_{TA} induced by different precipitation can be approximately 40.73% of the uncertainty in TRENDYv6 multi-model simulations induced by model structural and parameter uncertainty. Furthermore, we find a good linear relationship between global area-averaged land climatological annual precipitation and simulated total F_{TA}, implying more precipitation over land with stronger carbon sinks, especially over extra-tropical Northern Hemisphere (NH). For seasonal cycle, uncertainties in simulated F_{TA} over tropics plus extra-tropical southern hemisphere (Trop + SH) show relatively larger values in March-April-May and August-September-October. For interannual variability, uncertainties in simulated total F_{TA} are up to 40.61% (global), 38.17% (Trop + SH), and 29.63% (NH) of the TRENDYv6 inter-model uncertainty, respectively. In general, uncertainty in land precipitation data sets can cause considerable uncertainties

Key Points:

- Uncertainties in simulating land-atmosphere carbon fluxes (F_{TA}) on multiple time scales induced by different precipitation are investigated
- Uncertainties in climatology and interannual variability of global total F_{TA} are about 41% of uncertainties in TRENDYv6 simulations
- A good linear relationship emerges between global area-averaged land climatological annual precipitation and simulated total F_{TA}

Supporting Information:

Supporting Information may be found in the online version of this article.

Correspondence to:

J. Wang,
wangjun@nju.edu.cn

Citation:

Wang, M., Wang, J., Cai, Q., Zeng, N., Lu, X., Yang, R., et al. (2021). Considerable uncertainties in simulating land carbon sinks induced by different precipitation products. *Journal of Geophysical Research: Biogeosciences*, *126*, e2021JG006524. https://doi.org/10.1029/2021JG006524

Received 7 JUL 2021
Accepted 2 OCT 2021

Author Contributions:

Conceptualization: Meirong Wang, Jun Wang, Qixiang Cai, Ning Zeng
Formal analysis: Meirong Wang, Jun Wang
Writing – original draft: Meirong Wang, Jun Wang
Writing – review & editing: Xuehe Lu, Ruqi Yang, Fei Jiang, Hengmao Wang, Weimin Ju

in simulating F_{TA}, suggesting the importance of generating the better precipitation product for better simulating the terrestrial carbon sinks.

1. Introduction

The terrestrial biosphere model (TBM) is a useful tool for understanding the global and regional terrestrial carbon cycle. However, different model structures including processes considered and parameterizations and different forcing/boundary data sets, causing surprising differences in simulated responses of photosynthesis to CO_2 concentration, temperature, soil moisture, and vapor pressure deficit, result in large uncertainties in simulating terrestrial gross primary productivity (GPP) and net biome productivity (NBP) (Friedlingstein et al., 2006; Ito et al., 2017; Rogers, 2014; Rogers et al., 2014; Sitch et al., 2015).

In TRENDY intercomparison project, following the same experimental protocols, multiple state-of-the-art Dynamical Global Vegetation Models (DGVMs) are driven by the same climate forcing to simulate the global land carbon flux from terrestrial ecosystems to the atmosphere (F_{TA}, which equals to the negative value of NBP) (Sitch et al., 2015). The standard deviation of the annual C sink across these DGVMs is on average approximately 0.6 GtC yr^{-1} from 1959 to 2018 (Friedlingstein et al., 2019). This inter-model spread results mainly from the structural and parameter uncertainties, of which structural uncertainty is caused by the insufficient knowledge of how to represent the reality by the model, which tends to increase along with greater model complexity (Wieder et al., 2015). TBMs involved in the second phase of the Inter-Sectoral Impact Model Intercomparison Project (ISIMIP2a) were forced by four meteorological forcing data sets. Ito et al. (2017) suggested that their simulated global terrestrial GPP ranged from 98 to 141 GtC yr^{-1} during 1981–2000 with considerable inter-model and inter-data spreads. Therefore, besides the structural and parameter uncertainties, different meteorological forcing can cause the nonnegligible uncertainty in simulated terrestrial carbon fluxes by models.

It is well known that precipitation is one of the most critical meteorological forcing to drive the TBM. Precipitation, as the primary source of water for the land surface hydrological budget, to a large extent dominates the variations of soil moisture and terrestrial water storage (Humphrey et al., 2018) which play an important role in regulating terrestrial carbon fluxes on multiple time scales (climate extremes, interannual variability, etc.) (Humphrey et al., 2018, 2021; Wang, Jiang, et al., 2021; Wang, Wang, et al., 2021; Wang et al., 2016; Wang, Zeng, Wang, Jiang, Chen, et al., 2018; Wang, Zeng, Wang, Jiang, Wang, & Jiang, 2018; Zscheischler, Mahecha, et al., 2014; Zscheischler, Michalak, et al., 2014). The traditional reanalysis data sets have been widely used in terrestrial carbon simulations (J. M. Chen et al., 2012; Wang, Jiang, et al., 2021; Wang, Wang, et al., 2021) and in upscaling using the machine learning technique (Lu et al., 2021). Reanalysis data can be classified into three major categories according to the relative influence of the model and observations (Kalnay et al., 1996). Specifically, for example, the winds belong to the most reliable class because of their direct assimilation from observational data; humidity and surface temperature belong to the second class as they are the mixtures of the model results and observations; precipitation belongs to the third class which is derived from models. Therefore, precipitation data sets have large uncertainties, largely affecting the soil moisture simulations. The poor correlation coefficients between TBM simulated root zone soil moisture and satellite-derived terrestrial water storage variations are partially attributable to uncertainties of precipitation data (Humphrey et al., 2018). It is cautious for us to employ the precipitation data sets for climate analyses and TBM simulations. To constrain uncertainties in simulated soil moisture partially caused by precipitation data, many studies assimilated satellite-derived surface soil moisture into TBMs (Albergel et al., 2012; DeLannoy et al., 2014; Draper et al., 2012; Seo et al., 2021). Moreover, Scholze et al. (2016) and He et al. (2017) suggested that assimilation of satellite-derived soil moisture into TBMs can better simulate the terrestrial carbon cycle.

Although the multi-model simulations in ISIMIP2a were used to examine the uncertainties caused by different meteorological forcing data sets, they did not focus on the precipitation alone (Ito et al., 2017). Owing to the great influence of water availability on terrestrial carbon cycle and larger uncertainty in precipitation compared to other meteorological elements, it is necessary to comprehensively investigate to what extent precipitation alone can cause the uncertainty of NBP simulated by TBMs. Therefore, we in this study ran the state-of-the-art DGVM VEGAS to quantitatively examine the uncertainties in the simulated global and

Table 1
Eight Precipitation Data Sets Used in This Study to Drive VEGAS Simulations

Data sets	Time span	Resolution	References
CPC	1979–present	0.5° × 0.5°	M. Chen et al. (2008)
CRU TS4.04	1901–2019	0.5° × 0.5°	Harris et al. (2020)
Delaware v5.01	1900–2017	0.5° × 0.5°	Willmott and Matsuura (2001)
GPCC	1891–present	2.5° × 2.5°	Schneider et al. (2017)
PREC/L	1948–present	2.5° × 2.5°	M. Chen et al. (2002)
CAMS_OPI	1979–present	2.5° × 2.5°	Janowiak and Xie (1999)
CMAP	1979–present	2.5° × 2.5°	Xie and Arkin (1997)
GPCP v2.3	1979–present	2.5° × 2.5°	Adler et al. (2003)

regional NBP on climatology, seasonal cycle, and interannual variability, with VEGAS forced by eight precipitation products. Another important purpose is to provide the scientific evidence for VEGAS Near Real-Time (NRT) to select the most proper precipitation data set. Additionally, this research can provide some implications for the effect of soil moisture assimilations on the terrestrial carbon cycle.

This study is organized as follows: Section 2 will describe the precipitation data sets used here and experimental designs for VEGAS in detail. Section 3 will give out the results on climatology, seasonal cycle, and interannual variability. Discussion and concluding remarks will be presented in Sections 4 and 5, respectively.

2. Materials and Methods

2.1. Different Precipitation Products

In this study, we adopted eight precipitation products (Table 1) which were widely used in climate analyses to drive VEGAS simulations, in which five out of eight land precipitation data sets are produced from interpolation of gauge observations and the rest are the combination of satellite-based rainfall estimates and gauge observations. Brief introduction to these data sets is as follows:

1. NOAA Climate Prediction Center (CPC) Global Unified Gauge-Based Analysis of Daily Precipitation with its original resolution of 0.5° × 0.5° from 1979 to present (M. Chen et al., 2008). It is part of products from the CPC Unified Precipitation Project, whose primary goal is to generate a suite of unified precipitation products with consistent quantity and improved quality by integrating all information sources available at CPC and by means of the optimal interpolation (OI) objective analysis technique.
2. Climatic Research Unit (CRU) Time-Series (TS) version 4.04 of high resolution gridded data of month-by-month variation in climate from 1901 to 2019 (Harris et al., 2020). This data set was produced by CRU at the University of East Anglia and funded by the UK National Center for Atmospheric Science (NCAS), a NERC collaborative center, with the resolution of 0.5° × 0.5°. The CRU TS4.04 data were generated using angular-distance weighting (ADW) interpolation, based on monthly observations calculated from daily or sub-daily data by National Meteorological Services and other external agents.
3. University of Delaware Precipitation (Delaware v5.01) (Willmott & Matsuura, 2001). This data set has the resolution of 0.5° × 0.5° with monthly values from 1900 to 2017, produced from a large number of stations both from the Global Historical Climate Network, version 2 (GHCN2) and more extensively from the archive of Legates & Willmott. More complete description of the data can be accessed from their web pages at the University of Delaware.
4. Global Precipitation Climatology Center (GPCC) (Schneider et al., 2017). The data set used here is the Full Data Product (V2018) for the period 1891–2016 based on quality-controlled data from 67,200 stations worldwide that feature record durations of 10 years or longer and monitoring product for the period 2017 to present based on quality-controlled data from 7,000 stations. This product has a spatial resolution of 0.5° × 0.5°, 1.0° × 1.0°, and 2.5° × 2.5° latitude by longitude.
5. NOAA's PRECipitation REConstruction over Land (PREC/L) (M. Chen et al., 2002). This global analysis is defined by interpolation of gauge observations over land from over 17,000 stations collected in the

GHCN2 and the Climate Anomaly Monitoring System (CAMS) data sets with an OI technique of Gandin. Precipitation is available at 0.5° × 0.5°, 1.0° × 1.0°, and 2.5° × 2.5° latitude by longitude.

6. NOAA NCEP CAMS-outgoing longwave radiation precipitation index (CAMS_OPI) (Janowiak & Xie, 1999). This data set was produced from rain gauge data for land and OPI estimates for land points without observations and over the oceans, and was intended for real-time climate monitoring. Though authors strongly suggest that users adopt either the CMAP or GPCP for analyses, we here still employed this data set for the simulation because VEGAS NRT framework previously used this data set to construct the near real-time forcing data set (Wang, Zeng, Wang, Jiang, Wang, & Jiang, 2018).
7. CPC Merged Analysis of Precipitation (CMAP) (Xie & Arkin, 1997). The CMAP precipitation is obtained from five kinds of satellite estimates and gauge data, including a standard and enhanced version with NCEP Reanalysis from 1979 to present. We here used the standard version of CMAP with the resolution of 2.5° × 2.5°.
8. GPCP Version 2.3 Combined Precipitation Data Set (Adler et al., 2003). The GPCP product was produced from an integration of various satellite data sets over land and ocean and a gauge analysis over land with the resolution of 2.5° × 2.5° from 1979 to present. The combination of satellite-based rainfall estimates provides necessary spatial details to the rainfall analyses over land and the most complete analysis of rainfall over oceans.

2.2. VEGAS and Its Simulations

The state-of-the-art DGVM VEGAS, version 2.6, was used to investigate the uncertainty of simulated terrestrial NBP induced by different precipitation data sets. The introduction to its model structure and biological processes was described in the Appendix of Zeng, Mariotti, and Wetzel (2005). VEGAS model has been extensively involved in the Coupled Climate-Carbon Cycle Model Intercomparison Project (C^4MIP) (Friedlingstein et al., 2006), the TRENDY project (Sitch et al., 2015), and Multi-scale Synthesis and Terrestrial Model Intercomparison Project (MsTMIP) (Huntzinger et al., 2013). Its simulations have been widely used to understand the terrestrial carbon cycle upon climate extremes, seasonal cycle, interannual variability, and long-term trends (Wang et al., 2013; Wang, Zeng, Wang, Jiang, Wang, & Jiang, 2018; Zeng, Mariotti, et al., 2005; Zeng, Qian, et al., 2005; Zeng et al., 2014).

In this research, we investigated the impact of precipitation on F_{TA} which represents the terrestrial carbon sources and sinks. F_{TA} is the net carbon flux from terrestrial ecosystems into the atmosphere, calculated as

$$F_{TA} = -NBP = TER - GPP + D \tag{1}$$

where TER and GPP represent the total ecosystem respiration and photosynthesis, respectively. D represents the carbon flux induced by disturbances (mainly wildfires and harvest in VEGAS model). Its positive and negative values indicate carbon fluxes into the atmosphere (source) and into terrestrial ecosystems (sink), respectively.

In VEGAS simple-land, abbreviated "SLand," which is moderately more complicated than the bucket model (Zeng et al., 2000), the water budget in the whole soil layer that represents the root zone is

$$\frac{\partial W}{\partial t} = P - E - R + S \tag{2}$$

where W is the soil moisture content per unit area; P is the precipitation; E is the total evaporation; R is the total runoff, summed by surface and subsurface runoff; S represents the snowmelt. The soil can be saturated when W reaches the field capacity (W_0) which is dependent on surface types. Usefully, a relative soil wetness is defined in SLand,

$$w = W/W_o \tag{3}$$

where w will be unity at saturation. In the current version of the model, we use the following parameterization

$$\beta = w^{\alpha} \tag{4}$$

This nonlinear dependence of β on w takes effects of the soil moisture uptake by deep roots into account. The actual form of β is adopted according to observations and physically based parameterizations including heterogeneity effects (Zeng et al., 2000). We take the $\alpha = 0.5$ in VEGAS model now. The β is further used as

the water stress which influences vegetation photosynthesis in a colimiting function, heterotrophic respiration processes, and wildfire probability, hence influencing the variability of F_{TA} in Equation 1.

In this study, we ran VEGAS at the hourly time step with the 2.5° × 2.5° horizontal resolution, starting from the date of January 1, 1979. In detail, in the experimental protocols, we iterated VEGAS by just replacing the precipitation data sets (Table 1). For each simulation, we spun up VEGAS with constant meteorological drivers in 1979 for more than 500 years, in which we turned on the accelerator for soil carbon pools to reach equilibrium fast in the first 200 years. Hence, each simulation is independent. Except precipitation, the hourly temperature and radiation data sets are compiled from ECMWF Reanalysis v5 (ERA5) (Hersbach et al., 2020) and gridded cropland and pasture land use data are integrated from the History Database of the Global Environment (HYDE 3.2) (Klein Goldewijk et al., 2017).

2.3. F_{TA} in Comparison

For comparison, we in this study adopted 13 models simulated NBP ($-F_{TA}$) from the TRENDYv6 S3 simulation, in which the effects on the terrestrial carbon cycle of all the drivers, including CO_2, climate, and land use and land cover change, are taken into account (Sitch et al., 2015). The DGVMs include CABLE (Haverd et al., 2018), CLASS-CTEM (Melton & Arora, 2016), CLM4.5 (Oleson et al., 2013), ISAM (Jain et al., 2013), JSBACH (Reick et al., 2013), JULES (Clark et al., 2011), LPJ (Sitch et al., 2003), LPX-Bern (Keller et al., 2017), OCN (Zaehle et al., 2010), ORCHIDEE (Krinner et al., 2005), ORCHIDEE-MICT (Guimberteau et al., 2018), VEGAS (Zeng, Mariotti, & Wetzel, 2005), and VISIT (Kato et al., 2013). Additionally, an updated NEE-T inversion result from the Jena CarboScope, denoted as "sEXTocNEET_v2020" (Rodenbeck et al., 2018), was also employed.

2.4. Statistical Methods

For the interannual analysis, we applied the 12-month running average to de-seasonalize the monthly precipitation and F_{TA}. Then we used the Pearson's correlation coefficient to show their consistency. The Root Mean Square Error (RMSE) was used to quantify the discrepancies between simulated F_{TA} and sEXTocNEET_v2020 inversion result. The uncertainties induced by different precipitation products relative to TRENDYv6 multi-model simulations over different regions are calculated as

$$UNC = \frac{1}{n}\sum_{j}^{n}\frac{\sigma_j^{VEGAS}}{\sigma_j^{TRENDYv6}}\cdot 100\% \quad (5)$$

where σ_j^{VEGAS} represents the standard deviation for de-seasonalized VEGAS simulations forced by different precipitation in the jth month, and $\sigma_j^{TRENDYv6}$ represents the standard deviation in the same month for TRENDYv6 multi-model simulations. n denotes the number of available months in the analysis.

3. Results

3.1. Impacts of Precipitation Data on Climatological Annual F_{TA}

Figure 1 shows averages of climatological annual mean precipitation of eight different products and averages of annual mean F_{TA} simulated using these precipitation data sets. The heavier precipitation mainly occurs over the Tropics owing to the active convections, especially over Equatorial Asia and Amazon (Figure 1a). The heavy precipitation is strongly linked to the activity of global monsoon (Wang & Ding, 2008). These different precipitation data sets show the largest discrepancies in the low latitudes, especially over the northwest part of South America, central Africa, Equatorial Asia, and the Tibetan Plateau (Figure 1b). The simulated F_{TA} averaged from 1979 to 2016 shows obvious carbon uptake over the major crop regions (North America, Europe, India, and North China) and boreal forests and tundra areas in northern high latitudes. In the low latitudes, large areas show the positive F_{TA}, namely carbon release, mainly owing to the emissions of wildfires and land-use change, especially deforestation (Friedlingstein et al., 2019; van der Werf et al., 2017) (Figure 1c). Interestingly, the pattern of uncertainties in simulated F_{TA} induced by different precipitation data sets is obviously different from the pattern of discrepancies in precipitation (Figures 1d and 1b). Large uncertainties in simulated F_{TA} mainly occur in the transitional zones between

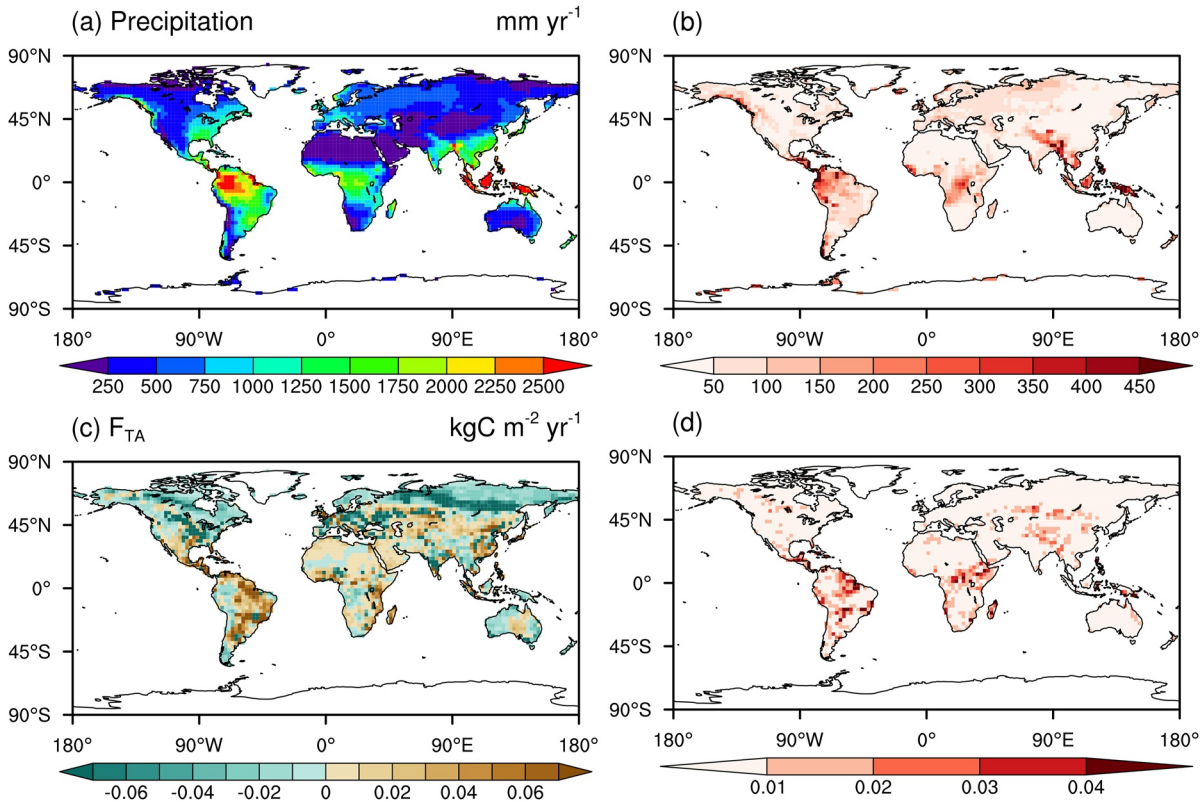

Figure 1. Averages (a) and standard deviations (b) of annual precipitation (mm yr^{-1}) of eight different precipitation data sets during 1979–2016. Averages (c) and standard deviations (d) of annual mean F_{TA} (kg C m^{-2} yr^{-1}) simulated using eight different precipitation data sets during 1979–2016.

tropical rainforests and savannas over South America and Africa and mid-latitude grasslands over Asia (Figure 1d). Different patterns of precipitation and F_{TA} discrepancies result from divergent sensitivities of vegetation over different regions to precipitation (Wang et al., 2016).

Given that there are no true values of precipitation and F_{TA} and CRU precipitation has been widely used in the TRENDY project, we here take the CRU precipitation and F_{TA} simulated using this precipitation data set as the references to display the Taylor diagrams for other precipitation and simulated F_{TA} (Figure 2). Consistently, the precipitation and their related F_{TA} show high spatial correlation coefficients (0.94–0.99) with the CRU and its F_{TA}, respectively. The CPC, CAMS_OPI, and CMAP show the relatively smaller standardized deviations (Figure 2a), whereas their related F_{TA} demonstrate the relatively higher standardized deviations (Figure 2b).

Figure 3 shows the associations between area-averaged climatological annual precipitation and their related simulated total F_{TA}. First of all, the amplitudes of F_{TA} simulated using VEGAS version 2.6 driven by CRU precipitation over different zones are within the TRENDYv6 inter-model spreads, implying that the VEGAS version 2.6 has at least the equivalent performance in simulating the terrestrial carbon sources and sinks compared to the other state-of-the-art DGVMs. Globally, the land precipitation has inter-data spreads from 702.78 (CPC) to 860.58 mm yr^{-1} (GPCP). It is worth mentioning that the integration of various satellite estimates and gauge observations do not make the land precipitation estimates converge. For example, there are obvious differences in CMAP and GPCP which are both widely used in climate analyses (Figure S1 in Supporting Information S1). These different precipitation data sets result in the different patterns of the simulated F_{TA} associated with their global total F_{TA} varying from −0.95 to −0.38 PgC yr^{-1} (Figures 3 and S2 in Supporting Information S1). Although this uncertainty in F_{TA} caused by different precipitation data sets is smaller than the uncertainty in TRENDYv6 multi-model simulations which is caused by the model structural and parameter uncertainty, their ratio ($\sigma_{precip}/\sigma_{TRENDYv6}$) can be up to approximately 40.73%.

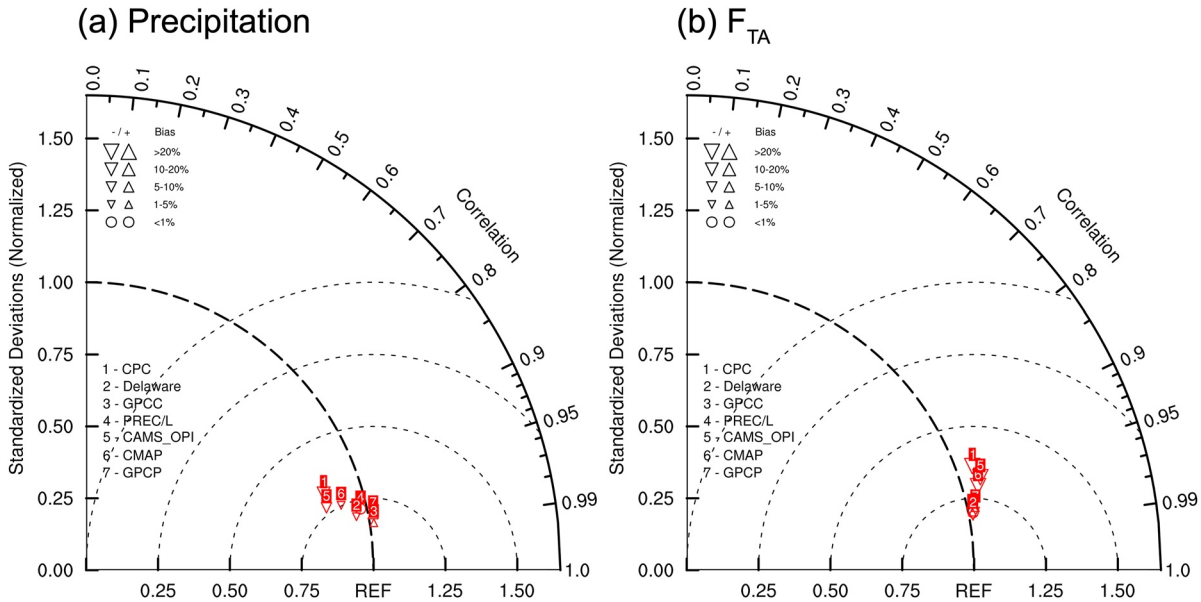

Figure 2. Taylor diagram for climatological precipitation and simulated F_{TA}. The CRU precipitation and F_{TA} simulated using this precipitation data set are taken as the references, given that CRU data sets were widely used in the TRENDY project.

Furthermore, a good linear relationship emerges between global area-averaged land annual precipitation and simulated total F_{TA} with a slope of −0.0040 Pg C yr^{-1} per mm yr^{-1} (R^2 = 0.58, p = 0.03). That is, the increase of 1 mm yr^{-1} in precipitation averaged over the global land can cause 0.0040 Pg C yr^{-1} more terrestrial carbon absorption.

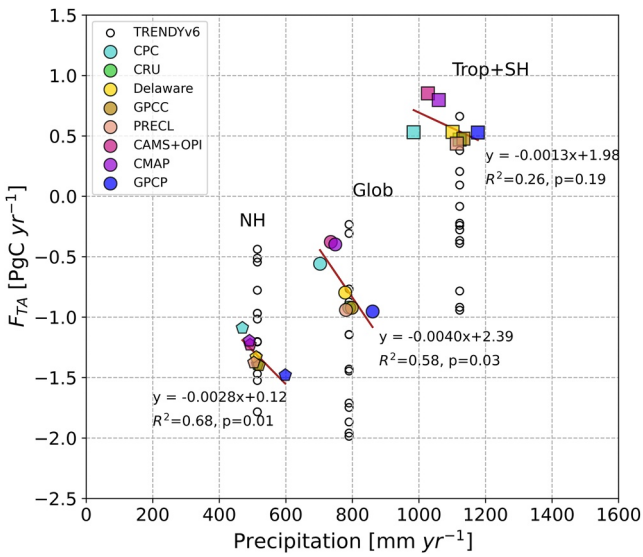

Figure 3. Associations between area-averaged climatological annual precipitation and simulated total F_{TA} over different zones. We separated global land regions into tropical plus southern extratropical regions (Trop + SH) and northern extratropical regions (NH). Simulations by individual Dynamical Global Vegetation Model (DGVM) in TRENDYv6 are also listed accordingly where the inter-model spreads are mainly caused by the model structural and parameter uncertainties. The precipitation and F_{TA} are in the units of mm yr^{-1} and Pg C yr^{-1}, respectively.

Separating the global land into tropical plus southern extratropical regions (Trop + SH) and northern extratropical regions (NH), we can comprehensively investigate the associations between precipitation and simulated F_{TA} in detail. Over the Trop + SH, the land precipitation has the uncertainty from 984.29 (CPC) to 1,177.20 mm yr^{-1} (GPCP). Except CAMS_OPI and CMAP, the total of simulated F_{TA} driven by other precipitation data sets is 0.50 ± 0.04 Pg C yr^{-1}. It is worth mentioning that though CPC has the smallest precipitation amplitude, the simulated F_{TA} has the almost same value compared to the GPCP which has the strongest precipitation amplitude. In contrast, smaller precipitation amplitudes of CAMS_OPI and CMAP cause the stronger carbon release here. These contrasting behaviors on one hand result from the spatial differences of precipitation patterns (Figure S1 in Supporting Information S1) and vegetation sensitivities to precipitation (or soil moisture) (Jung et al., 2017; Wang et al., 2016). On the other hand, different precipitation as climate drivers for VEGAS simulations can cause different states of the terrestrial carbon cycle, that is, differences in amplitudes of GPP, TER, vegetation, and soil carbon pools. Hence, the association between different precipitation and simulated F_{TA} shows a weaker linear relationship with the slope of −0.0013 Pg C yr^{-1} per mm yr^{-1} (R^2 = 0.26, p = 0.19). The uncertainty of F_{TA} relative to TRENDYv6 multi-model simulations is approximately 31.50%.

Over NH, the simulated F_{TA} amplitudes suggest a stronger sensitivity to different precipitation with the slope of −0.0028 Pg C yr^{-1} per mm yr^{-1} (R^2 = 0.68, p = 0.01) than the behavior over Trop + SH. This sensitivity accounts for 70% of the relationship between global total simulated F_{TA} and precipitation. Though precipitation over NH has relatively smaller

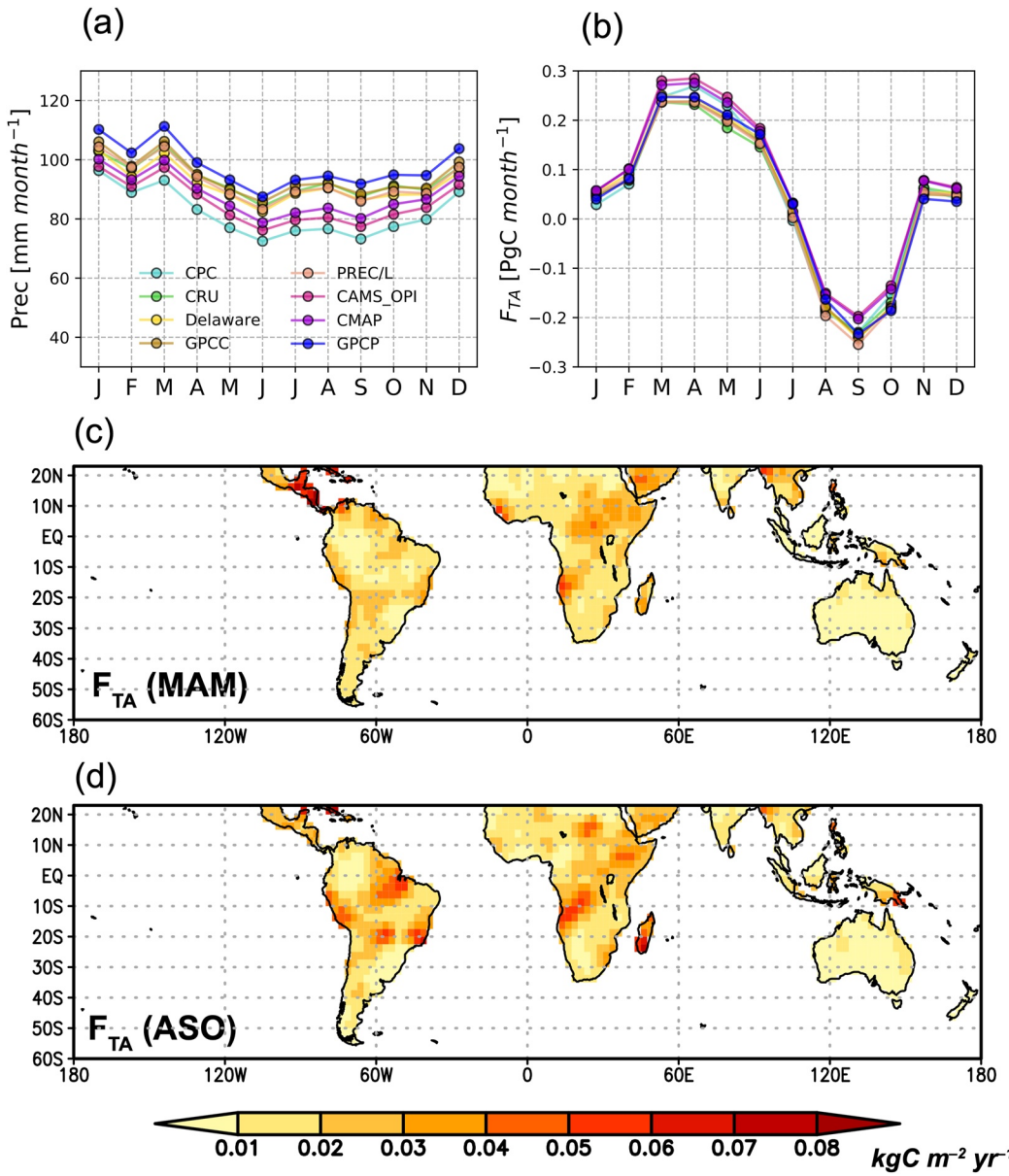

Figure 4. Seasonal variations of simulated F_{TA} over Trop + SH with the related different land precipitation. (a) Precipitation (mm month^{-1}), (b) tropical F_{TA} (PgC month^{-1}), (c) standard deviation of F_{TA} during March-April-May (MAM), and (d) standard deviation of F_{TA} during August-September-October (ASO) with the unit of kg C m^{-2} yr^{-1}.

inter-data spread from 469.43 (CPC) to 598.11 mm yr^{-1} (GPCP), the simulated F_{TA} show differences from −1.09 to −1.48 Pg C yr^{-1} with the σ = 0.12 PgC yr^{-1} (approximately 30.32% of TRENDYv6 multi-model simulations).

3.2. Impacts of Precipitation Data on the Seasonal Cycle in F_{TA}

Owing to the large seasonal cycle amplitude of F_{TA} over NH, uncertainties of simulated F_{TA} by different precipitation products are insignificant. Hence, we mainly focus on the impact of different precipitation on seasonal variations in F_{TA} over Trop + SH (Figure 4). Different precipitation products keep nearly constant inter-data spreads during the entire seasonal cycle (Figure 4a). However, uncertainties in their corresponding simulated F_{TA} show the obvious seasonal differences with the relatively larger uncertainties during March-April-May (MAM) and August-September-October (ASO) (Figure 4b). Spatially, the largest

uncertainties mainly happen over regions north to the Equator (Northern Africa) during MAM (Figure 4c), but over regions south to the Equator (South America and Africa) during ASO (Figure 4d).

In climatological seasonal evolution, during MAM, the soil moisture is relatively low over Northern Africa because the precipitation mainly locates in Southern Hemisphere (Figure S3a in Supporting Information S1), making the carbon releases here (Figures S3b and S4a in Supporting Information S1). During ASO, the rain-belts locate over the equatorial Northern Hemisphere. Low precipitation lasting from preceding months makes the soil moisture relatively low over the regions south to the Equator (Figure S3a in Supporting Information S1), resulting in the carbon releases from the Equator to 20°S (Figure S3b in Supporting Information S1), mainly over South America and Southern Africa (Figure S4b in Supporting Information S1). Therefore, the large differences in simulated F_{TA} generally occur when the tropical regions are in their dry seasons, implying that tropical ecosystems are phenologically more sensitive to water availability during dry seasons than during wet seasons.

3.3. Impacts of Precipitation Data on the Interannual Variability in F_{TA}

On the interannual time scale, many literatures have reported that precipitation (or soil moisture) played a vital role in the interannual variability of the global and regional terrestrial carbon cycle (Humphrey et al., 2018, 2021; Wang, Jiang, et al., 2021; Wang, Wang, et al., 2021; Wang, Zeng, Wang, Jiang, Chen, et al., 2018; Wang, Zeng, Wang, Jiang, Wang, & Jiang, 2018; Zeng, Mariotti, & Wetzel, 2005). The interannual variations of different land precipitation and their correlation coefficients in pairs are presented in Figure 5. It is clear that the discrepancies among different land precipitation products keep in year-to-year variations, implying that systematic biases exist in different precipitation products, causing the differences in climatological annual precipitation (Figure 3). However, the interannual variations of precipitation show the high consistency on the global and regional scales (Figures 5a, 5c, and 5e). The precipitation has the much stronger interannual variability over Trop + SH than over NH (Figures 5c and 5e), showing less precipitation during El Niño events and more precipitation during La Niña events which largely contributes to the interannual variability of the terrestrial carbon cycle (Wang et al., 2016; Wang, Zeng, Wang, Jiang, Chen, et al., 2018; Zeng, Mariotti, & Wetzel, 2005).

Specifically, over Trop + SH, except CPC and CAMS_OPI, other precipitation data sets are more consistent on the interannual time scale, showing the correlation coefficients in pairs in the range from 0.81 to 0.97 ($p < 0.05$) (Figure 5d). In contrast, larger discrepancy occurs over NH (Figure 5f). Higher correlation coefficients in pairs (>0.81) occur among CRU, Delaware, GPCC, and GPCP. Globally, we can find that data sets of CRU, Delaware, GPCC, PREC/L, and GPCP are more consistent with the higher correlation coefficients in pairs (>0.81, Figure 5b). In contrast, CPC, CAMS_OPI, and CMAP show the lower correlation coefficients with the other products.

Differences in precipitation amplitudes and variations can result in the uncertainty in simulating the interannual variability of the terrestrial carbon cycle. Figure 6 shows the interannual variations of simulated F_{TA} associated with their uncertainties relative to the TRENDYv6 multi-model simulations. TRENDYv6 multi-model simulations indicate that the global F_{TA} interannual variability is dominated by the tropical F_{TA} rather than the F_{TA} over NH, with the anomalous carbon release induced by widespread dry and warm conditions during El Niño events and the anomalous carbon uptake due to wet and cool conditions during La Niña events (Figures 6b and 6c), as suggested by previous studies (Bousquet et al., 2000; Wang et al., 2016; Zeng, Mariotti, & Wetzel, 2005). The anomalous terrestrial carbon releases can obviously lag El Niño events or show no lags, which were determined by types of El Niños (Wang, Zeng, Wang, Jiang, Chen, et al., 2018). By comparison, VEGAS has the good performance in simulating the interannual variability of F_{TA}, with the correlation coefficients of 0.49 for global total, 0.62 for Trop + SH, and 0.55 for NH ($p < 0.05$) between TRENDYv6 ensemble mean and ensemble mean of VEGAS simulations (Figures 6b and 6c).

On the interannual time scale, relative to the inter-model uncertainties in TRENDYv6, uncertainties in VEGAS simulations induced by different precipitation are, albeit smaller, nonnegligible (Figures 6b–6d). According to Equation 5, the uncertainty for the global total simulated F_{TA} induced by different precipitation can be up to 40.61% of the TRENDYv6 inter-model uncertainty (Figure 6a). Over the different latitudinal

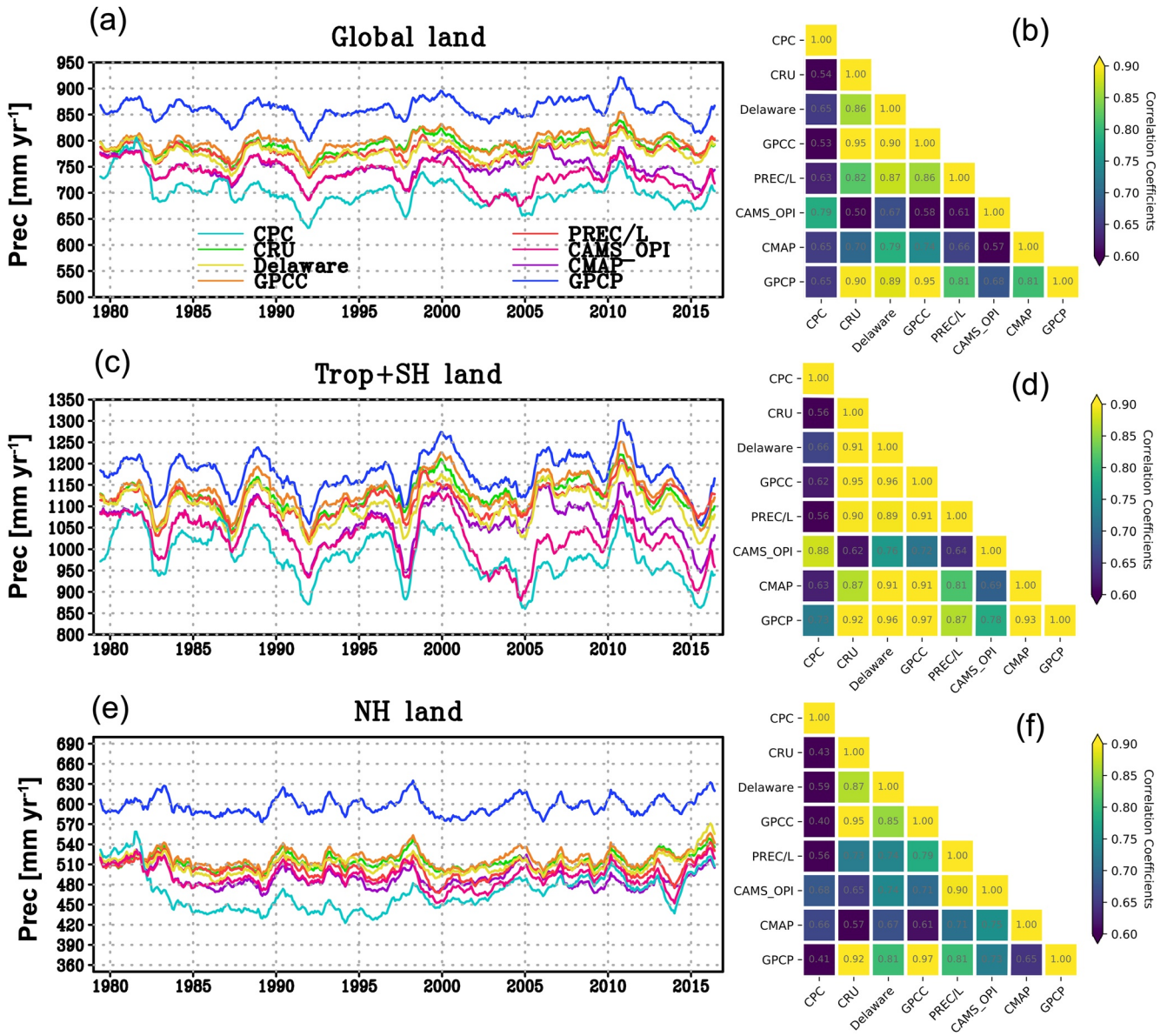

Figure 5. Interannual variations of different land precipitation and their correlation coefficients in pairs. (a, c, and e) Area-averaged land precipitation over globe, Trop + SH, and NH, respectively. (b, d, and f) Pearson's correlation coefficients in pairs. The time series here are de-seasonalized by the 12-month running average with the unit of mm yr^{-1}.

regions, relative uncertainty over Trop + SH is obviously stronger than that over NH, with their corresponding 38.17% and 29.63% of the TRENDYv6 inter-model uncertainties, respectively.

Though there are no "true" values for the interannual variability in F_{TA}, we take the updated NEE-T inversion result ("sEXTocNEET") from the Jena CarboScope (Rodenbeck et al., 2018) as a reference because the inversion result can to a large extent capture the large-scale interannual carbon variability after directly assimilating the CO_2 observations at stations. Regardless of the structural and parameter uncertainty of VEGAS model, direct comparisons between simulated F_{TA} forced by different precipitation and NEE-T inversion result are presented in Figure 7. Although their interannual variations are basically consistent (Figure 7a), differences exist (Figure 7b). Clearly, the largest RMSE occurs between F_{TA} forced by CPC and NEE-T, whereas the RMSE between F_{TA} forced by PREC/L and NEE-T is smallest, which implies that the PREC/L is a better alternative than originally used CAMS_OPI in VEGAS NRT framework (Wang, Zeng, Wang, Jiang, Wang, & Jiang, 2018). Except CPC, the RMSE between simulated F_{TA} forced by other

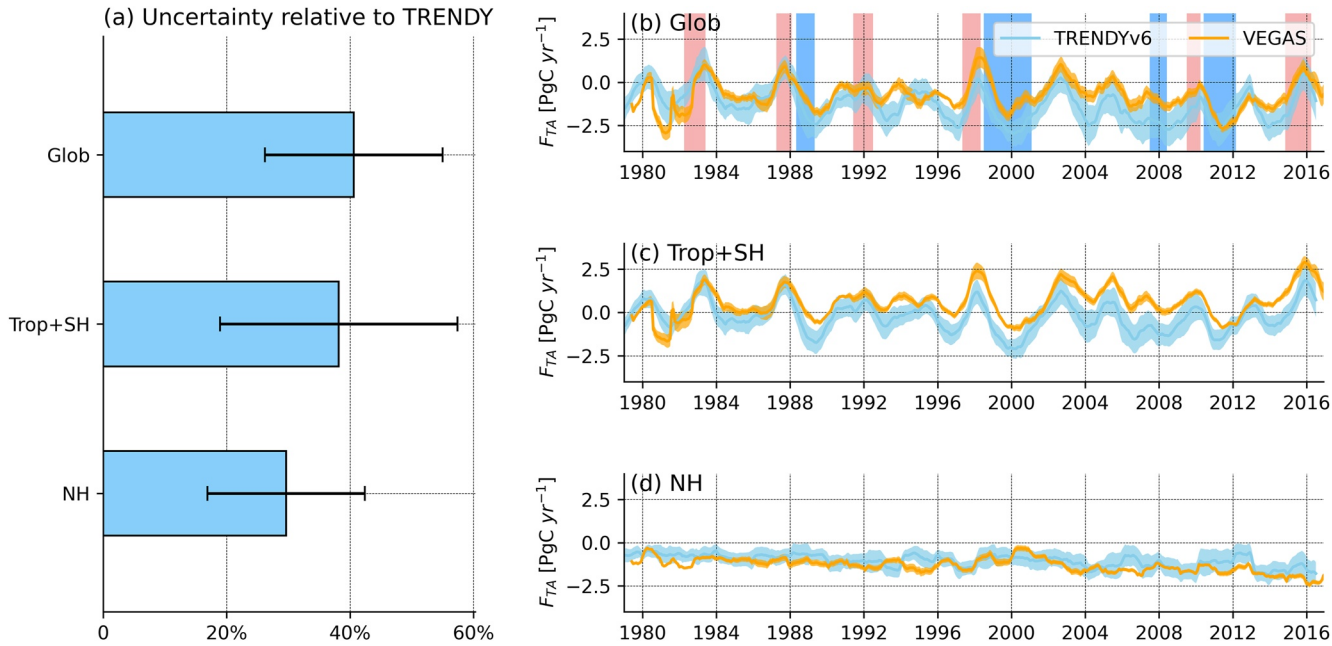

Figure 6. Interannual variations of simulated F_{TA} associated with their uncertainties relative to the mean of 13 TRENDYv6 models forced by same meteorological data and experimental protocols. (a) Averaged uncertainties relative to TRENDYv6 over globe, Trop + SH, and NH. The error bars represent the one-σ of the relative uncertainties. (b, c, and d) Interannual variations of VEGAS and TRENDYv6 simulated F_{TA} over globe, Trop + SH, and NH. The light coral and dodger blue shaded areas in (b) represent the strong El Niño and La Niña events, respectively, which were defined based on the Oceanic Niño Index (ONI).

gauge-based precipitation products and NEE-T are close. However, it is worth mentioning that the integration of satellite and gauge estimates does not further reduce the uncertainties in land precipitation (CMAP and GPCP) (Figures 3 and 5) associated with resultant F_{TA} (Figures 3 and 7).

4. Discussions

The results discussed in this study are simulations by VEGAS. As we know, focusing on the terrestrial hydrological cycle, although under the same protocols and climatological drivers, the simulated variations of terrestrial root zone soil moisture by different DGVMs indicate low correlation coefficients (Humphrey et al., 2018). Additionally, different model structures, including processes considered and parameterizations, and so on, can cause surprising differences in model representation of responses of photosynthesis to CO_2 concentration, temperature, soil moisture, and atmospheric vapor pressure deficit (Rogers, 2014; Rogers et al., 2014; Wang et al., 2016). Therefore, different models may suggest different results to some extent under these different precipitation data sets.

This research can also give some implications for carbon assimilations. Parazoo et al. (2014) constrained the global distribution of GPP by using an optimal estimation approach with the a priori mean and uncertainty derived from an ensemble of DGVMs in TRENDY project. As this research and Ito et al. (2017) indicated that apart from inter-model spreads in the carbon cycle simulations induced by the structural and parameter uncertainty, uncertainty in climatological drivers can also cause, albeit smaller, nonnegligible spreads of carbon fluxes. Hence, they may underestimate the background errors by taking the uncertainty derived from TRENDY multi-model simulations, which was mainly induced by structural and parameter uncertainty since these models were driven by the same meteorological data set. Underestimation in background errors in data assimilation can largely bias the posterior results. Additionally, precipitation to a large extent dominates the variations of soil moisture and terrestrial water storage (Humphrey et al., 2018). And here it is clear that different precipitation products can cause considerable uncertainty in simulating F_{TA} on the climatological, seasonal, and interannual time scales, more specifically regulated by the root zone soil moisture in VEGAS model. In satellite era, assimilating satellite-observed soil moisture into TBMs can constrain the hydrological cycle simulations in models (Mladenova et al., 2020; Seo et al., 2021). Hence, this

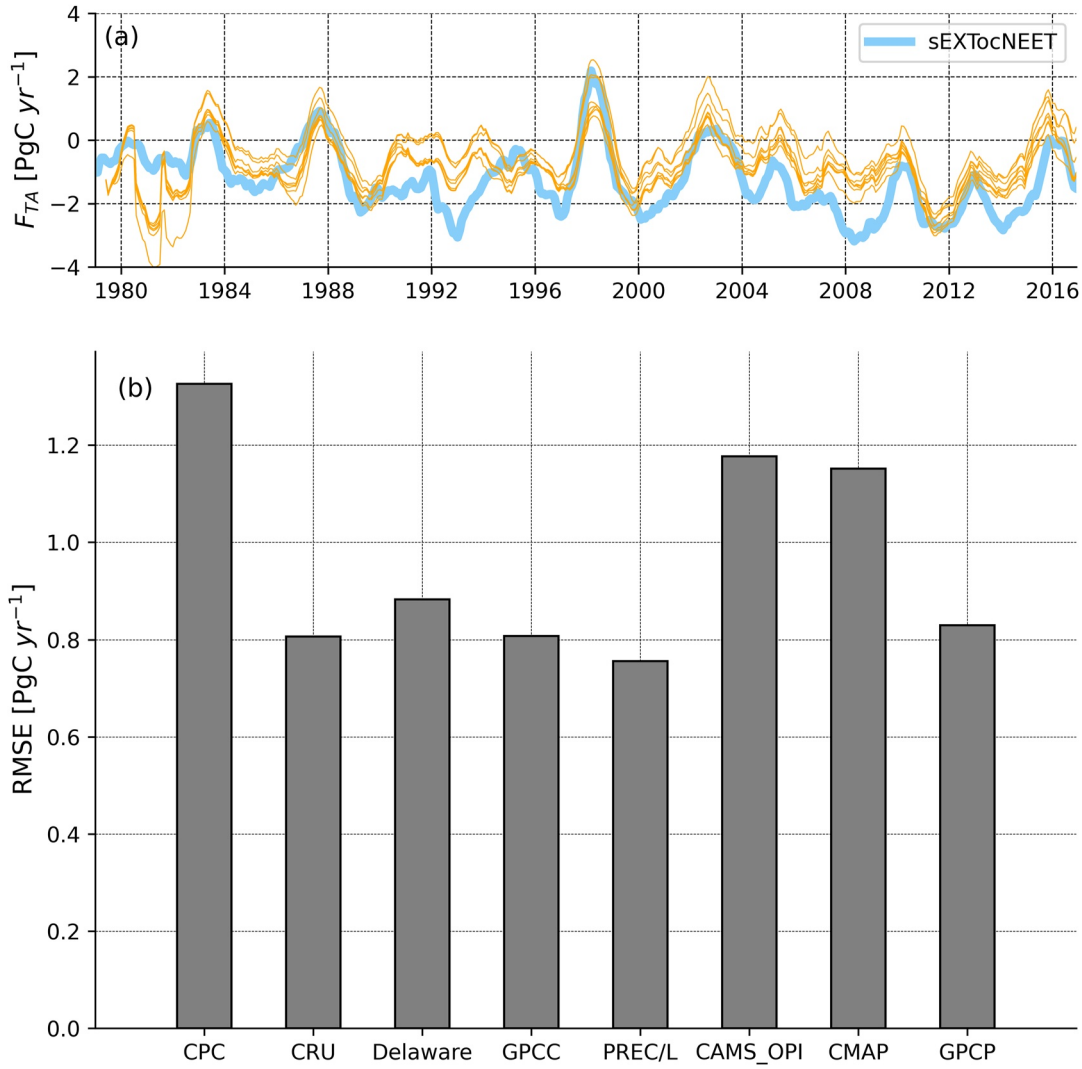

Figure 7. Root Mean Square Errors (RMSE) of simulated F_{TA} relative to atmospheric inversion results of Jena CarboScope sEXTocNEET_v2020. (a) Time series of interannual variabilities of the simulated F_{TA} forced by different precipitation products (orange lines) and Jena CarboScope NEE-T inversion result (blue line). (b) RMSE of individual simulated F_{TA} relative to the results of Jena CarboScope.

considerable uncertainty in simulated F_{TA} induced by the uncertainty in precipitation may be reduced to some extent by assimilating satellite-observed soil moisture. Several studies have also shown the effectiveness of assimilating satellite-observed soil moisture on simulating the global terrestrial carbon cycle (He et al., 2017; Scholze et al., 2016). For example, Scholze et al. (2016) indicated that assimilating SMOS L3 soil moisture can considerably reduce the uncertainty for both regional net ecosystem productivity and net primary productivity. He et al. (2017) suggested the significant improvement in GPP simulations over the single-cropping agricultural lands by assimilating the Soil Moisture Active Passive (SMAP) satellite measurements into a process-based ecosystem model.

Furthermore, we have demonstrated that a significant linear relationship exists between different climatological annual precipitation and simulated total F_{TA} over NH, showing the slope of −0.0028 PgC yr^{-1} per mm yr^{-1} ($R^2 = 0.68$, $p = 0.01$) (Figure 3). It implies that regardless of other environmental condition changes, more precipitation can result in stronger land carbon sinks over NH. On the basis of CMIP5 simulations, future precipitation over NH will likely increase (Collins et al., 2013). Hence, increased precipitation, warmed temperature, and rising atmospheric CO_2 concentration might altogether enhance the land carbon sinks over NH in the future, though there is an uncertainty in the carbon losses in permafrost (Ciais et al., 2013).

5. Conclusion

In this study, we comprehensively investigated to what extent precipitation alone can cause uncertainties in simulating terrestrial carbon sources and sinks, by using eight precipitation products to drive the VEGAS model. Main conclusions are summarized below.

On climatology, owing to divergent water sensitivities of vegetation over different regions, the geographical distribution of uncertainties in simulated F_{TA} differs from the pattern of discrepancies in precipitation. The uncertainty in simulated global total F_{TA} induced by different precipitation is approximately 40.73% of the uncertainty in TRENDYv6 multi-model simulated F_{TA}, which is mainly induced by the model structural and parameter uncertainty. Furthermore, we find a good linear relationship between global area-averaged land climatological annual precipitation and simulated total F_{TA} with the slope of -0.0040 Pg C yr^{-1} per mm yr^{-1} ($R^2 = 0.58$, $p = 0.03$), in which sensitivity over NH to precipitation accounts for 70%. This linear relationship implies that more land precipitation might induce the increase of land carbon sinks.

For seasonal cycle, over the Trop + SH, compared to the nearly constant inter-precipitation spreads, uncertainties in corresponding simulated F_{TA} show obvious seasonal differences with the relatively larger uncertainties in MAM and ASO, phenologically showing that ecosystems are more sensitive to the water availability during dry seasons than during wet seasons over the certain regions.

For interannual variability, VEGAS has the good performance in simulating the interannual variability of F_{TA}. Uncertainties in simulated total F_{TA} are, albeit smaller, nonnegligible, which are up to 40.61% (global), 38.17% (Trop + SH), and 29.63% (NH) of the TRENDYv6 inter-model uncertainty, respectively. Additionally, comparisons between simulated F_{TA} forced by different precipitation and NEE-T inversion result suggest that the PREC/L can be a better alternative than originally used CAMS_OPI in VEGAS NRT framework.

Data Availability Statement

CPC Global Unified Precipitation data, Delaware v5.01, GPCC, PREC/L, CMAP, GPCP Version 2.3 are provided by the NOAA/OAR/ESRL PSL, Boulder, Colorado, USA, from their Web site at https://psl.noaa.gov/data/gridded/tables/precipitation.html. CRU TS4.04 precipitation is from https://catalogue.ceda.ac.uk/uuid/89e1e34ec3554dc98594a5732622bce9. And CAMS_OPI precipitation is provided at https://www.cpc.ncep.noaa.gov/products/global_precip/html/wpage.cams_opi.html. The TRENDY DGVMs data are available at https://sites.exeter.ac.uk/trendy. VEGAS simulations for the findings of this article can be accessed in the figshare repository at https://figshare.com/articles/dataset/Considerable_uncertainties_in_simulating_land_carbon_sinks_induced_by_different_precipitation_products/16614277.

Acknowledgments
The authors gratefully acknowledge the TRENDY DGVM community, as part of the Global Carbon Project, for access to gridded land data. This study was supported by the National Natural Science Foundation of China (41807434), the National Key R&D Program of China (2020YFA0607504), and Fundamental Research Funds for the Central Universities (0904-14380028). The authors are grateful to the High Performance Computing Center (HPCC) of Nanjing University for doing the numerical calculations in this paper on its blade cluster system.

References

Adler, R. F., Huffman, G. J., Chang, A., Ferraro, R., Xie, P. P., Janowiak, J., et al. (2003). The version-2 global precipitation climatology project (GPCP) monthly precipitation analysis (1979-present). *Journal of Hydrometeorology*, *4*(6), 1147–1167. https://doi.org/10.1175/1525-7541(2003)004<1147:tvgpcp>2.0.co;2

Albergel, C., de Rosnay, P., Gruhier, C., Munoz-Sabater, J., Hasenauer, S., Isaksen, L., et al. (2012). Evaluation of remotely sensed and modelled soil moisture products using global ground-based in situ observations. *Remote Sensing of Environment*, *118*, 215–226. https://doi.org/10.1016/j.rse.2011.11.017

Bousquet, P., Peylin, P., Ciais, P., Le Quere, C., Friedlingstein, P., & Tans, P. P. (2000). Regional changes in carbon dioxide fluxes of land and oceans since 1980. *Science*, *290*(5495), 1342–1346. https://doi.org/10.1126/science.290.5495.1342

Chen, J. M., Mo, G., Pisek, J., Liu, J., Deng, F., Ishizawa, M., & Chan, D. (2012). Effects of foliage clumping on the estimation of global terrestrial gross primary productivity. *Global Biogeochemical Cycles*, *26*. https://doi.org/10.1029/2010gb003996

Chen, M., Shi, W., Xie, P., Silva, V. B. S., Kousky, V. E., Wayne Higgins, R., & Janowiak, J. E. (2008). Assessing objective techniques for gauge-based analyses of global daily precipitation. *Journal of Geophysical Research*, *113*(D4). https://doi.org/10.1029/2007jd009132

Chen, M., Xie, P., Janowiak, J. E., & Arkin, P. A. (2002). Global land precipitation: A 50-yr monthly analysis based on gauge observations. *Journal of Hydrometeorology*, *3*, 249–266. https://doi.org/10.1175/1525-7541(2002)003<0249:glpaym>2.0.co;2

Ciais, P., Sabine, C., Bala, G., Bopp, L., Brovkin, V., Canadell, J., et al. (2013). Carbon and other biogeochemical cycles. In T. F. Stocker, D. Qin, G.-K. Plattner, M. Tignor, S. K. Allen, J. Boschung, A. Nauels, Y. Xia, V. Bex, & P. M. Midgley (Eds.), *Climate Change 2013: The Physical Science Basis. Contribution of Working Group I to the Fifth Assessment Report of the Intergovernmental Panel on Climate Change*. Cambridge University Press.

Clark, D. B., Mercado, L. M., Sitch, S., Jones, C. D., Gedney, N., Best, M. J., et al. (2011). The Joint UK Land Environment Simulator (JULES), model description—Part 2: Carbon fluxes and vegetation dynamics. *Geoscientific Model Development*, *4*(3), 701–722. https://doi.org/10.5194/gmd-4-701-2011

Collins, M., Knutti, R., Arblaster, J., Dufresne, J.-L., Fichefet, T., Friedlingstein, P., et al. (2013). Long-term climate change: Projections, commitments and irreversibility. In T. F. Stocker, D. Qin, G.-K. Plattner, M. Tignor, S. K. Allen, J. Boschung, A. Nauels, Y. Xia, V. Bex, & P. M. Midgley (Eds.), *Climate Change 2013: The Physical Science Basis. Contribution of Working Group I to the Fifth Assessment Report of the Intergovernmental Panel on Climate Change*. Cambridge University Press.

DeLannoy, G. J. M., Koster, R. D., Reichle, R. H., Mahanama, S. P. P., & Liu, Q. (2014). An updated treatment of soil texture and associated hydraulic properties in a global land modeling system. *Journal of Advances in Modeling Earth Systems*, *6*(4), 957–979. https://doi.org/10.1002/2014ms000330

Draper, C. S., Reichle, R. H., De Lannoy, G. J. M., & Liu, Q. (2012). Assimilation of passive and active microwave soil moisture retrievals. *Geophysical Research Letters*, *39*. https://doi.org/10.1029/2011gl050655

Friedlingstein, P., Cox, P., Betts, R., Bopp, L., Von Bloh, W., Brovkin, V., et al. (2006). Climate-carbon cycle feedback analysis: Results from the C(4)MIP model intercomparison. *Journal of Climate*, *19*(14), 3337–3353. https://doi.org/10.1175/jcli3800.1

Friedlingstein, P., Jones, M. W., O'Sullivan, M., Andrew, R. M., Hauck, J., Peters, G. P., et al. (2019). Global Carbon Budget 2019. *Earth System Science Data*, *11*(4), 1783–1838.

Guimberteau, M., Zhu, D., Maignan, F., Huang, Y., Yue, C., Dantec-Nédélec, S., et al. (2018). ORCHIDEE-MICT (v8.4.1), a land surface model for the high latitudes: Model description and validation. *Geoscientific Model Development*, *11*(1), 121–163. https://doi.org/10.5194/gmd-11-121-2018

Harris, I., Osborn, T. J., Jones, P., & Lister, D. (2020). Version 4 of the CRU TS monthly high-resolution gridded multivariate climate dataset. *Scientific Data*, *7*(1), 109. https://doi.org/10.1038/s41597-020-0453-3

Haverd, V., Smith, B., Nieradzik, L., Briggs, P. R., Woodgate, W., Trudinger, C. M., et al. (2018). A new version of the CABLE land surface model (Subversion revision r4601) incorporating land use and land cover change, woody vegetation demography, and a novel optimisation-based approach to plant coordination of photosynthesis. *Geoscientific Model Development*, *11*(7), 2995–3026. https://doi.org/10.5194/gmd-11-2995-2018

He, L., Chen, J. M., Liu, J., Bélair, S., & Luo, X. (2017). Assessment of SMAP soil moisture for global simulation of gross primary production. *Journal of Geophysical Research: Biogeosciences*, *122*(7), 1549–1563. https://doi.org/10.1002/2016jg003603

Hersbach, H., Bell, B., Berrisford, P., Hirahara, S., Horányi, A., Muñoz-Sabater, J., et al. (2020). The ERA5 global reanalysis. *Quarterly Journal of the Royal Meteorological Society*, *146*(730), 1999–2049. https://doi.org/10.1002/qj.3803

Humphrey, V., Berg, A., Ciais, P., Gentine, P., Jung, M., Reichstein, M., et al. (2021). Soil moisture–atmosphere feedback dominates land carbon uptake variability. *Nature*, *592*(7852), 65–69. https://doi.org/10.1038/s41586-021-03325-5

Humphrey, V., Zscheischler, J., Ciais, P., Gudmundsson, L., Sitch, S., & Seneviratne, S. I. (2018). Sensitivity of atmospheric CO_2 growth rate to observed changes in terrestrial water storage. *Nature*, *560*(7720), 628–631. https://doi.org/10.1038/s41586-018-0424-4

Huntzinger, D. N., Schwalm, C., Michalak, A. M., Schaefer, K., King, A. W., Wei, Y., et al. (2013). The North American Carbon Program Multi-Scale Synthesis and Terrestrial Model Intercomparison Project – Part 1: Overview and experimental design. *Geoscientific Model Development*, *6*(6), 2121–2133. https://doi.org/10.5194/gmd-6-2121-2013

Ito, A., Nishina, K., Reyer, C. P. O., Francois, L., Henrot, A. J., Munhoven, G., et al. (2017). Photosynthetic productivity and its efficiencies in ISIMIP2a biome models: Benchmarking for impact assessment studies. *Environmental Research Letters*, *12*(8). https://doi.org/10.1088/1748-9326/aa7a19

Jain, A. K., Meiyappan, P., Song, Y., & House, J. I. (2013). CO_2 emissions from land-use change affected more by nitrogen cycle, than by the choice of land-cover data. *Global Change Biology*, *19*(9), 2893–2906. https://doi.org/10.1111/gcb.12207

Janowiak, J. E., & Xie, P. P. (1999). CAMS-OPI: A global satellite-rain gauge merged product for real-time precipitation monitoring applications. *Journal of Climate*, *12*(11), 3335–3342. https://doi.org/10.1175/1520-0442(1999)012<3335:coagsr>2.0.co;2

Jung, M., Reichstein, M., Schwalm, C. R., Huntingford, C., Sitch, S., Ahlstrom, A., et al. (2017). Compensatory water effects link yearly global land CO_2 sink changes to temperature. *Nature*, *541*(7638), 516–520. https://doi.org/10.1038/nature20780

Kalnay, E., Kanamitsu, M., Kistler, R., Collins, W., Deaven, D., Gandin, L., et al. (1996). The NCEP/NCAR 40-year reanalysis project. *Bulletin of the American Meteorological Society*, *77*(3), 437–471. https://doi.org/10.1175/1520-0477(1996)077<0437:tnyrp>2.0.co;2

Kato, E., Kinoshita, T., Ito, A., Kawamiya, M., & Yamagata, Y. (2013). Evaluation of spatially explicit emission scenario of land-use change and biomass burning using a process-based biogeochemical model. *Journal of Land Use Science*, *8*(1), 104–122. https://doi.org/10.1080/1747423x.2011.628705

Keller, K. M., Lienert, S., Bozbiyik, A., Stocker, T. F., Churakova, O. V., Frank, D. C., et al. (2017). 20th century changes in carbon isotopes and water-use efficiency: Tree-ring-based evaluation of the CLM4.5 and LPX-Bern models. *Biogeosciences*, *14*(10), 2641–2673. https://doi.org/10.5194/bg-14-2641-2017

Klein Goldewijk, K., Beusen, A., Doelman, J., & Stehfest, E. (2017). Anthropogenic land use estimates for the Holocene—HYDE 3.2. *Earth System Science Data*, *9*(2), 927–953. https://doi.org/10.5194/essd-9-927-2017

Krinner, G., Viovy, N., de Noblet-Ducoudre, N., Ogee, J., Polcher, J., Friedlingstein, P., et al. (2005). A dynamic global vegetation model for studies of the coupled atmosphere-biosphere system. *Global Biogeochemical Cycles*, *19*(1). https://doi.org/10.1029/2003gb002199

Lu, H., Li, S., Ma, M., Bastrikov, V., Chen, X., Ciais, P., et al. (2021). Comparing machine learning-derived global estimates of soil respiration and its components with those from terrestrial ecosystem models. *Environmental Research Letters*, *16*(5). https://doi.org/10.1088/1748-9326/abf526

Melton, J. R., & Arora, V. K. (2016). Competition between plant functional types in the Canadian Terrestrial Ecosystem Model (CTEM) v.2.0. *Geoscientific Model Development*, *9*(1), 323–361. https://doi.org/10.5194/gmd-9-323-2016

Mladenova, I. E., Bolten, J. D., Crow, W., Sazib, N., & Reynolds, C. (2020). Agricultural drought monitoring via the assimilation of SMAP soil moisture retrievals into a Global Soil Water Balance Model. *Frontiers in Big Data*, *3*, 10. https://doi.org/10.3389/fdata.2020.00010

Oleson, K., Lawrence, D., Bonan, G., Drewniak, B., Huang, M., Koven, C., et al. (2013). Technical Description of version 4.5 of the Community Land Model (CLM). NCAR.

Parazoo, N. C., Bowman, K., Fisher, J. B., Frankenberg, C., Jones, D. B., Cescatti, A., et al. (2014). Terrestrial gross primary production inferred from satellite fluorescence and vegetation models. *Global Change Biology*, *20*(10), 3103–3121. https://doi.org/10.1111/gcb.12652

Reick, C. H., Raddatz, T., Brovkin, V., & Gayler, V. (2013). Representation of natural and anthropogenic land cover change in MPI-ESM. *Journal of Advances in Modeling Earth Systems*, *5*(3), 459–482. https://doi.org/10.1002/jame.20022

Rodenbeck, C., Zaehle, S., Keeling, R., & Heimann, M. (2018). How does the terrestrial carbon exchange respond to inter-annual climatic variations? A quantification based on atmospheric CO_2 data. *Biogeosciences*, *15*, 2481–2498. https://doi.org/10.5194/bg-15-2481-2018

Rogers, A. (2014). The use and misuse of V(c,max) in Earth System Models. *Photosynthesis Research*, *119*(1–2), 15–29. https://doi.org/10.1007/s11120-013-9818-1

Rogers, A., Medlyn, B. E., & Dukes, J. S. (2014). Improving representation of photosynthesis in Earth System Models. *New Phytologist*, *204*, 12–14. https://doi.org/10.1111/nph.12972

Schneider, U., Finger, P., Meyer-Christoffer, A., Rustemeier, E., Ziese, M., & Becker, A. (2017). Evaluating the hydrological cycle over land using the Newly-Corrected Precipitation Climatology from the Global Precipitation Climatology Centre (GPCC). *Atmosphere*, *8*(3). https://doi.org/10.3390/atmos8030052

Scholze, M., Kaminski, T., Knorr, W., Blessing, S., Vossbeck, M., Grant, J. P., & Scipal, K. (2016). Simultaneous assimilation of SMOS soil moisture and atmospheric CO_2 in-situ observations to constrain the global terrestrial carbon cycle. *Remote Sensing of Environment*, *180*, 334–345. https://doi.org/10.1016/j.rse.2016.02.058

Seo, E., Lee, M. I., & Reichle, R. H. (2021). Assimilation of SMAP and ASCAT soil moisture retrievals into the JULES land surface model using the Local Ensemble Transform Kalman Filter. *Remote Sensing of Environment*, 253. https://doi.org/10.1016/j.rse.2020.112222

Sitch, S., Friedlingstein, P., Gruber, N., Jones, S. D., Murray-Tortarolo, G., Ahlström, A., et al. (2015). Recent trends and drivers of regional sources and sinks of carbon dioxide. *Biogeosciences*, *12*(3), 653–679. https://doi.org/10.5194/bg-12-653-2015

Sitch, S., Smith, B., Prentice, I. C., Arneth, A., Bondeau, A., Cramer, W., et al. (2003). Evaluation of ecosystem dynamics, plant geography and terrestrial carbon cycling in the LPJ dynamic global vegetation model. *Global Change Biology*, *9*(2), 161–185. https://doi.org/10.1046/j.1365-2486.2003.00569.x

van der Werf, G. R., Randerson, J. T., Giglio, L., van Leeuwen, T. T., Chen, Y., Rogers, B. M., et al. (2017). Global fire emissions estimates during 1997–2016. *Earth System Science Data*, *9*(2), 697–720. https://doi.org/10.5194/essd-9-697-2017

Wang, B., & Ding, Q. (2008). Global monsoon: Dominant mode of annual variation in the tropics. *Dynamics of Atmospheres and Oceans*, *44*(3–4), 165–183. https://doi.org/10.1016/j.dynatmoce.2007.05.002

Wang, J., Bao, Q., Ning, Z., Liu, Y. M., Wu, G. X., & Ji, D. Y. (2013). Earth System Model FGOALS-s2: Coupling a dynamic global vegetation and terrestrial carbon model with the physical climate system model. *Advances in Atmospheric Sciences*, *30*(6), 1549–1559. https://doi.org/10.1007/s00376-013-2169-1

Wang, J., Jiang, F., Wang, H., Qiu, B., Wu, M., He, W., et al. (2021). Constraining global terrestrial gross primary productivity in a global carbon assimilation system with OCO-2 chlorophyll fluorescence data. *Agricultural and Forest Meteorology*, 304–305. https://doi.org/10.1016/j.agrformet.2021.108424

Wang, J., Wang, M., Kim, J. S., Joiner, J., Zeng, N., Jiang, F., et al. (2021). Modulation of land photosynthesis by the Indian Ocean Dipole: Satellite-based observations and CMIP6 future projections. *Earth's Future*, *9*(4). https://doi.org/10.1029/2020ef001942

Wang, J., Zeng, N., & Wang, M. (2016). Interannual variability of the atmospheric CO_2 growth rate: Roles of precipitation and temperature. *Biogeosciences*, *13*(8), 2339–2352. https://doi.org/10.5194/bg-13-2339-2016

Wang, J., Zeng, N., Wang, M., Jiang, F., Chen, J., Friedlingstein, P., et al. (2018). Contrasting interannual atmospheric CO2 variabilities and their terrestrial mechanisms for two types of El Ninos. *Atmospheric Chemistry and Physics*, *18*, 10333–10345. https://doi.org/10.5194/acp-18-10333-2018

Wang, J., Zeng, N., Wang, M., Jiang, F., Wang, H., & Jiang, Z. (2018). Contrasting terrestrial carbon cycle responses to the 1997/98 and 2015/16 extreme El Niño events. *Earth System Dynamics*, *9*(1), 1–14. https://doi.org/10.5194/esd-9-1-2018

Wieder, W. R., Cleveland, C. C., Lawrence, D. M., & Bonan, G. B. (2015). Effects of model structural uncertainty on carbon cycle projections: Biological nitrogen fixation as a case study. *Environmental Research Letters*, *10*(4). https://doi.org/10.1088/1748-9326/10/4/044016

Willmott, C. J., & Matsuura, K. (2001). *Terrestrial air temperature and precipitation: Monthly and annual time series (1950 – 1999)*. Retrieved from http://climate.geog.udel.edu/~climate/html_pages/README.ghcn_ts2.html

Xie, P. P., & Arkin, P. A. (1997). Global precipitation: A 17-year monthly analysis based on gauge observations, satellite estimates, and numerical model outputs. *Bulletin of the American Meteorological Society*, *78*(11), 2539–2558. https://doi.org/10.1175/1520-0477(1997)078<2539:gpayma>2.0.co;2

Zaehle, S., Friend, A. D., Friedlingstein, P., Dentener, F., Peylin, P., & Schulz, M. (2010). Carbon and nitrogen cycle dynamics in the O-CN land surface model: 2. Role of the nitrogen cycle in the historical terrestrial carbon balance. *Global Biogeochemical Cycles*, *24*. https://doi.org/10.1029/2009gb003522

Zeng, N., Mariotti, A., & Wetzel, P. (2005). Terrestrial mechanisms of interannual CO_2 variability. *Global Biogeochemical Cycles*, *19*(1), GB1016. https://doi.org/10.1029/2004gb002273

Zeng, N., Neelin, J. D., & Chou, C. (2000). A quasi-equilibrium tropical circulation model—Implementation and simulation. *Journal of the Atmospheric Sciences*, *57*, 1767–1796. https://doi.org/10.1175/1520-0469(2000)057<1767:aqetcm>2.0.co;2

Zeng, N., Qian, H. F., Roedenbeck, C., & Heimann, M. (2005). Impact of 1998-2002 midlatitude drought and warming on terrestrial ecosystem and the global carbon cycle. *Geophysical Research Letters*, *32*(22). https://doi.org/10.1029/2005gl024607

Zeng, N., Zhao, F., Collatz, G. J., Kalnay, E., Salawitch, R. J., West, T. O., & Guanter, L. (2014). Agricultural Green Revolution as a driver of increasing atmospheric CO_2 seasonal amplitude. *Nature*, *515*(7527), 394–397. https://doi.org/10.1038/nature13893

Zscheischler, J., Mahecha, M. D., von Buttlar, J., Harmeling, S., Jung, M., Rammig, A., et al. (2014). A few extreme events dominate global interannual variability in gross primary production. *Environmental Research Letters*, *9*(3). https://doi.org/10.1088/1748-9326/9/3/035001

Zscheischler, J., Michalak, A. M., Schwalm, C., Mahecha, M. D., Huntzinger, D. N., Reichstein, M., et al. (2014). Impact of large-scale climate extremes on biospheric carbon fluxes: An intercomparison based on MsTMIP data. *Global Biogeochemical Cycles*, *28*(6), 585–600. https://doi.org/10.1002/2014gb004826